High-Temperature Treatment of Li-Rich Cathode Materials with Ammonia: Improved Capacity and Mean Voltage Stability during Cycling

*Evan M. Erickson, Hadar Sclar, Florian Schipper, Jing Liu, Ruiyuan Tian, Chandan Ghanty, Larisa Burstein, Nicole Leifer, Judith Grinblat, Michael Talianker, Ji-Yong Shin, Jordan K. Lampert, Boris Markovsky, Anatoly I. Frenkel, and Doron Aurbach**

Li-rich electrode materials of the family $xLi_2MnO_3\cdot(1-x)LiNi_aCo_bMn_cO_2$ ($a+b+c=1$) suffer a voltage fade upon cycling that limits their utilization in commercial batteries despite their extremely high discharge capacity, ≈250 mA h g^{-1}. Li-rich, $0.35Li_2MnO_3\cdot0.65LiNi_{0.35}Mn_{0.45}Co_{0.20}O_2$, is exposed to NH_3 at 400 °C, producing materials with improved characteristics: enhanced electrode capacity and a limited average voltage fade during 100 cycles in half cells versus Li. Three main changes caused by NH_3 treatment are established. First, a general bulk reduction of Co and Mn is observed via X-ray photoelectron spectroscopy and X-ray absorption near edge structure. Next, a structural rearrangement lowers the coordination number of Co—O and Mn—O bonds, as well as formation of a surface spinel-like structure. Additionally, Li^+ removal from the bulk causes the formation of surface LiOH, Li_2CO_3, and Li_2O. These structural and surface changes can enhance the voltage and capacity stability of the Li-rich material electrodes after moderate NH_3 treatment times of 1–2 h.

Dr. E. M. Erickson, Dr. H. Sclar, Dr. F. Schipper, Dr. R. Tian, Dr. C. Ghanty, Dr. N. Leifer, Dr. J. Grinblat, Prof. B. Markovsky, Prof. D. Aurbach
Department of Chemistry
Faculty of Exact Sciences
Bar-Ilan University
Ramat-Gan 5290002, Israel
E-mail: Doron.Aurbach@biu.ac.il

Dr. J. Liu, Prof. A. I. Frenkel
Department of Materials Science and Chemical Engineering
Stony Brook University
Stony Brook, NY 11794, USA

Dr. L. Burstein
Wolfson Applied Materials Research Center
Tel-Aviv University
Tel-Aviv 69978, Israel

Prof. M. Talianker
Department of Materials Engineering
Ben Gurion University of the Negev
Beer-Sheva 8410501, Israel

Dr. J.-Y. Shin, Dr. J. K. Lampert
BASF SE
67063 Ludwigshafen am Rhein, Rheinland-Pfalz, Germany

The ORCID identification number(s) for the author(s) of this article can be found under https://doi.org/10.1002/aenm.201700708.

DOI: 10.1002/aenm.201700708

1. Introduction

Since the discovery by Thackeray and Rossouw in 1991 that acid could activate Li_2MnO_3,[1] followed by the discovery by Gopukumar and co-workers in 1999 that this inactive phase could be activated electrochemically,[2] interest in integrated Li_2MnO_3 and composite phases has grown rapidly.[3] The Li_2MnO_3 phase can deliver a high theoretical capacity based on Li extraction of ≈460 mA h g^{-1}, though practical realities limit the total extracted capacity to ≈100 mA h g^{-1}, often with rapid capacity decay.[4] Attempts at stabilizing this material through lattice doping or forming "composites" with alternative materials mirrored struggles seen in the layered transition metal (TM) oxide field. For instance, $LiNiO_2$ suffers Ni^{2+} mixing in the Li^+ layer that causes dramatically different capacities for different synthesis parameters,[5] and $LiMnO_2$ does not easily form a layered *R-3m* structure,[6] rather forming the orthorhombic phase, *pmnm* with a zig-zag structure that causes low rate capability and capacity.[7] Incorporation of other Co, Mn, or Ni into pure lithiated transition metal oxides alleviated problems found with the pure, single $LiTMO_2$ materials.[8] Using a similar strategy, integration of Li_2MnO_3 with layered $LiMO_2$ and spinel components produced electrode materials that could perform >300 mA h g^{-1} discharge capacity reversibly.[3,9] Subsequent patent applications were granted to Thackeray and co-workers on integrated materials containing Li_2MnO_3 and both the layered TM oxides[10] and with spinel material.[11]

Integrated $xLi_2MnO_3\bullet yLiNi_aCo_bMn_cO_2$ ($x+y=1$, $a+b+c=1$) (Li-rich) materials are of particular interest since they have large, stable capacities above 250 mA h g^{-1}, though initial charging during the activation step can reach much higher, even up to >500 mA h g^{-1}.[12,13] Activation is a complex process involving oxygen release, Li_2O extraction, and the formation of surface spinel.[13–15] The spinel-phase domains formed can prevent to some extent further oxygen release from the bulk of the material during cycling, something which the material is susceptible to since it is believed that along with TMs, O^{2-} acts as a

charge acceptor.[16–19] Indeed, when the activation step is slowed or performed at lower temperatures so that electrode's passivation is improved, subsequent discharge capacities of Li-rich electrodes are enhanced.[20] Voltage fading of Li-rich cathodes is not primarily caused by improper surface passivation or spinel formation however; a progressive trapping of TM ions that inactivate their redox couples and impedes Li^+ reinsertion into the TM layer is the primary driver of Li-rich material electrodes' voltage and capacity fading during cycling.[21–23] This voltage fade remains the largest barrier for the commercialization of Li-rich materials.[22,24]

Recently, Dahn and co-workers demonstrated improved capacity of spinel materials through treatment with ammonia, which acts as a reducing agent to yield oxygen-deficient $Li(Li_{0.33}Mn_{1.67})O_{4-\delta}$ compounds.[25] Further performance enhancement of Li-rich material was shown by Meng and co-workers, who exposed Li-rich material to NH_4HCO_3 at high temperatures, and used differential electrochemical mass spectrometry (DEMS) to show that surface oxygen vacancies on these materials improved electrode capacity and rate capability, though the authors attributed the creation of oxygen vacancies to reaction with CO_2 produced from NH_4HCO_3 decomposition.[26] Another group suggested that the reaction mechanism of NH_3 treatment resulted in some sort of nitridation of the surface, confirmed through energy-dispersive X-ray spectroscopy (EDX) line scans and X-ray photoelectron spectroscopy (XPS) peaks, though very low nitrogen peak intensity was observed.[27] XPS studies of cathode materials exposed to NH_3 showed that an acid–base reaction could occur between the TM oxides and NH_3, forming a $M-NH_2$ surface species and transferring the proton to the oxide to form a hydroxide, though this was an unstable compound formed in situ at high vacuum.[28]

The purpose of this paper was to study the impact of ammonia on the structure and surface of Li-rich cathode materials in solid–gas reactions and to characterize the extent that NH_3 pretreatment may improve the overall capacity, as well as stabilize the capacity and average voltage fading of these cathodes during cycling of Li-cells. We also aimed to elucidate a mechanism by which ammonia reacts with the lithiated transition metal oxides, to establish an optimal duration of the thermal reaction, and to analyze why NH_3-treated materials show improved cathode performance. To our knowledge, the above issues were studied for the first time.

2. Results and Discussion

For clarity, this section is arranged by grouping various data by observation and conclusions they generate. First, a justification for the study based on the enhanced electrochemical performance of Li-rich materials treated with NH_3 is presented. The effects of NH_3 treatment are then explored, beginning evidence from XPS and X-ray absorption near edge structure (XANES) that NH_3 treatment causes a bulk reduction of transition metals of the Li-rich material. This is followed by XPS, Raman, and extended X-ray absorption fine structure (EXAFS) indications that structural reorganization occurs due to NH_3 treatment. Finally, evidence for Li^+ extraction and generation of various lithium salts is presented from XPS, X-ray diffraction (XRD), and electron diffraction studies. A summary of the results describing the effects of NH_3 treatment on Li-rich materials is then provided.

2.1. Enhanced Electrochemical Performance of Li-Rich Cathode Materials by NH_3 Treatment

Figure 1A depicts the discharge capacities for untreated (black) and 1 h (red), 2 h (blue), and 4 h (green) NH_3-treated Li-rich electrodes, as well as rate capabilities measured from *C*/15 to 4*C*. We have established that 1 h NH_3 treatment improved rate capability, especially at high rates of 2*C* and 4*C*, and can be considered as optimal time for increasing capacity at these rates. However, the 2 h treatment has no effect, and the 4 h

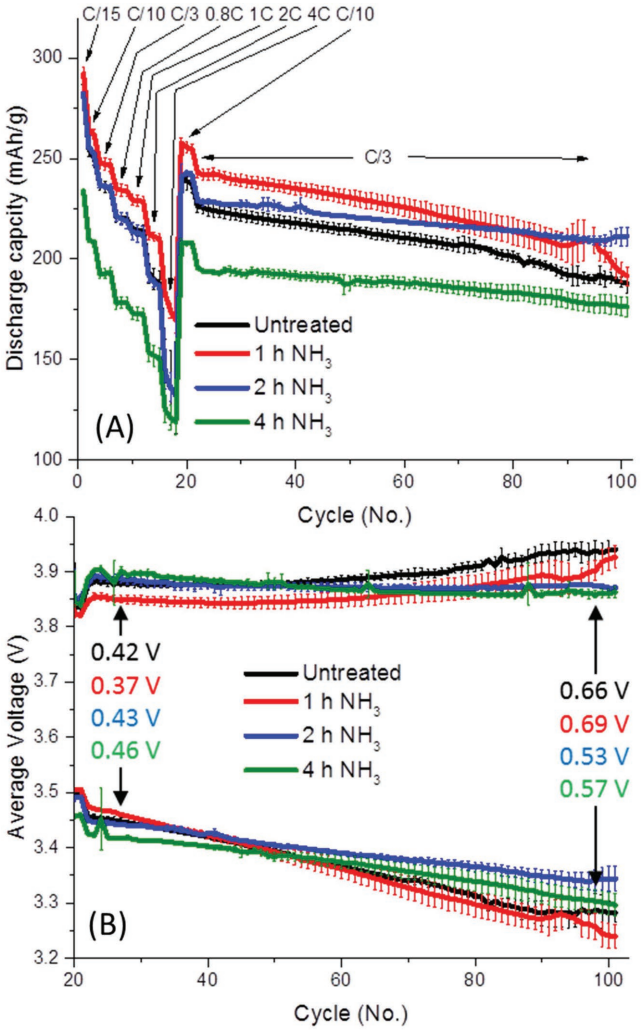

Figure 1. A) Discharge capacity and B) average voltage evolution in charge and discharge measured during cycling from electrodes comprising NH_3-treated and untreated Li-rich $0.35Li_2MnO_3{\cdot}0.65LiNi_{0.35}Mn_{0.45}Co_{0.20}O_2$ materials (as marked). The difference between average charge and discharge voltages are indicated by each materials respective color. Three to four coin cells were averaged for each data set, giving error bars based on one standard deviation. The average voltages are only plotted from the constant rate, *C*/3, cycles for clarity.

treatment worsens rate performance slightly. Clearly different effects are at play with NH_3 treatment, namely, at shorter treatment times (1 h), the discharge capacity and rate capability increase. Another effect that occurs after longer NH_3 treatment (2 and 4 h) causes the electrode's average voltage stability to be enhanced, though this effect interferes with the rate capability and discharge capacity at longer treatment times.

After the initial rate capability measurements (Figure 1A), cycling stability at a constant rate, $C/3$, was measured. It was established that 1 h of NH_3 treatment increases discharge capacity by ≈20 mA h g^{-1}, though it fades rapidly after 50 cycles, while after 2 h of treatment the capacity stabilizes substantially, compared to the untreated material. The calculated values of the capacity fade over 60 cycles for the untreated and 2 h NH_3-treated materials are ≈0.42 and ≈0.25 mA h g^{-1} $cycle^{-1}$, respectively. It is evident that 4 h treatment with ammonia results in much lower discharge capacities. Thus, we considered 2 h as an optimal treatment time at 400 °C for stabilizing the discharge capacity of Li-rich cathodes, and we have focused on characterization of the 2 h NH_3-treated sample over that of the 1 h NH_3-treated sample. This condition is also optimal for decreasing and stabilizing the mean voltage difference $\delta V = V_{ch} - V_{disch}$ upon cycling, as demonstrated in Figure 1B, although δV is minimal at the beginning of cycling for 1 h treated samples. Note that this parameter was shown to be an important characteristic for stabilizing the cycling performance of Li-rich high-energy cathodes in Li-ion batteries.[29]

The first cycle data with the voltage profiles and derivative capacity dq/dV plots are presented in **Figure 2**A,B, respectively. The redox reactions designations for the peaks 1–5 in Figure 2B for Li-rich materials are complex and the subject of controversy, with many overlapping and different processes. Peak 1 in Figure 2B is ascribed to extraction of Li^+ from the Li^+ layer, $Ni^{2+/4+}$ and $Co^{3+/4+}$ oxidation similar to normal layered structure (*R-3m* space group), Ni-rich compounds, for example, $LiNi_{0.8}Co_{0.1}Mn_{0.1}O_2$.[15,30–32] An intense peak 2 at a potential >4.5 V (not shown in order to maintain the *Y*-axis scale for the other peaks) corresponds to the electrochemical activation of the material.[19,33,34] This is a complex reaction beyond the scope of this paper, believed to involve Li^+ extraction from the TM layer, partial migration of TMs to the Li^+ layer as Li^+ is depleted, O^{2-} oxidation resulting in O_2 evolution from the materials' surface, and the formation of surface MnO_2.[19,33,34] As a result of activation, the reversible redox processes of $Mn^{3+/4+}$, along with reversible charge acceptance by O^{2-} anions occur.[15,31] Interesting new work on Li-rich analogue materials have suggested that the reversible charge acceptance by O^{2-} anions occurs via formation of a peroxo-dimer species, though there are other competing theories on the nature of O^{2-} charge acceptance.[16,17,19,35] Due to the electrochemical activation, reversible Li^+ extraction from the TM layer is possible, and whether Li^+ inserts into the Li layer or the TM layer can be easily tracked via in situ X-ray diffraction through the monitoring evolution of the *c*-lattice parameter.[15,31] As it follows from Figure 2B, reduction peaks 3, 1_{Red}, and 4 are believed to reflect Li^+ insertion into the TM layer, whereas peak 5 is probably related to Li^+ insertion into the Li^+ layer.[15,30,31] Overall, for this paper we will refer to the work by Yu et al. for peak designations; according to their interpretation, peak 3 involves O^{2-x} reduction, peak 1_{Red} involves Ni and Co reduction, and peaks 4 and 5 are related to reduction of $Mn^{4+/3+}$ involving Li^+ insertion into the TM layer and the Li^+ layer, respectively.[30] We have established that ammonia treatment dramatically affects the process of Li^+ insertion into the TM and Li^+ layers reflected by peaks 4 and 5, respectively, as the NH_3 treatments are lengthened. Since peaks 4 and 5 correspond to the $Mn^{4+/3+}$ reduction with Li^+ insertion to the TM and lithium layers, respectively, the NH_3 treatment seems to predominately affect the Li_2MnO_3 domains of the Li-rich material.[15,30] Peak 4 (Li^+ insertion into the TM layer) seems to be shifted to lower potentials, whereas peak 5 (Li^+ insertion into the Li layer) seems to be shifted to higher potentials. Peaks shifting to lower potentials and their broadening

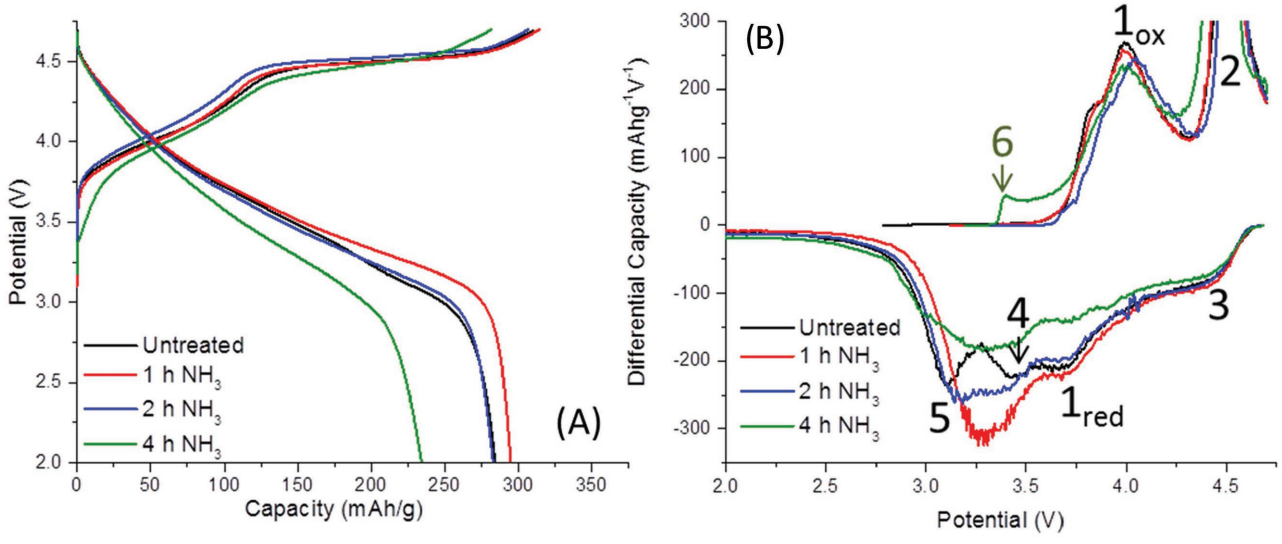

Figure 2. A) Voltage profiles and B) differential capacity (dq/dV) plots versus voltage of first cycles of electrodes prepared from untreated and NH_3-treated Li-rich materials.

are indicative of slower kinetics, suggesting the NH_3 treatment increases Li^+ insertion kinetics for the Li layer at the expense of the TM layer.

One of the most interesting features in Figure 2B is an additional oxidation peak, labeled 6 that arises after 4 h NH_3 treatment. It may relate to the possible reduction by NH_3 treatment of some transition metals that are reoxidized during charge, or peak 6 reflects corresponding oxidation processes in the range of 3–3.5 V (peaks 4 and 5), which only occur after electrode activation, or after Mn^{4+} reduction.

2.2. Further Evidence for Bulk Reduction by NH_3 Treatment: XPS and XANES Studies

Figure 3 represents the XPS Mn 3s and Mn 2p spectra of the untreated and 2 and 4 h NH_3-treated materials. The Mn 3s peak is split due to a coupling with the 3d valence band.[36] Peak splitting of the Mn 3s multiplet is changed slightly from 4.75 eV on the pristine sample to 4.60 eV on the 2 h NH_3-treated sample and 5.00 eV on the 4 h NH_3-treated sample, suggesting the appearance of Mn components with oxidation state lower than 4+ after 4 h NH_3 treatment. This is in correlation with the oxidation peak 6 (green) observed in the first cycle of the 4 h NH_3-treated material depicted in Figure 2B. Further evidence for the reduction of Mn in the 4 h NH_3-treated material is observed in the Mn $2p_{3/2}$ peak that shifts to lower binding energy and becomes broader (Figure 3B).

The Co, Ni, and Mn K-edge XANES spectra for untreated and 4 h NH_3-treated materials are presented in **Figure 4**. These spectra are dominated by the transition of a 1s core electron to an unoccupied 4p bound state and are therefore sensitive to the local atomic and electronic structure of absorbing atoms. Each spectrum contains a main peak, known as the "white line." The intensity and position of the white line are directly related to the occupancy of the p-states and, indirectly, to the charge state of the material. The XANES spectra at Co and Mn K-edges in Figure 4A and C show a decrease in white line intensity and shift to lower energies corresponding to reduction after NH_3 treatment. The Ni K-edge spectra, however, do not change after NH_3 treatment. The absorption edge positions, defined by the first inflection point of the absorption edge (vide supra), may be correlated with standards, including metal foils and oxides, to estimate the average charge state of the corresponding absorbing atoms in the material.[37] Using this correlation, we observed that the NH_3 treatment resulted in an average bulk reduction of Mn from 3.3 to 3.1 and a reduction of Co from 3.8 to 3.7. As observed by the lack of peak shift for the Ni K-edge in Figure 4B, no reduction of Ni was observed.

2.3. Evidence for Structural Changes after NH_3 Treatment

Not only transition metal ion reduction was observed after NH_3 treatment but also some surface structural changes of Li-rich materials were established. **Figure 5** depicts the XPS Ni 2p and Co 2p spectra of untreated, 2 and 4 h NH_3-treated Li-rich material. Similar to the XANES data depicted in Figure 4, the Ni 2p XPS structure does not show any reduction after NH_3 treatment but in opposite shifts to higher binding energies. This shift however may not necessarily be related to oxidation, but possibly a conversion to $Ni(OH)_2$ surface species which show a $2p_{3/2}$ peak around 855.6 eV.[38] The Co 2p XPS structure demonstrates a slight shift to higher binding energies after 4 h of NH_3 treatment, indicating a higher oxidation state, in contradiction to that of XANES data. This is likely due to the fact that XPS is a surface technique whereas XANES is a bulk ensemble technique. Many surface reorganizations that can alter transition

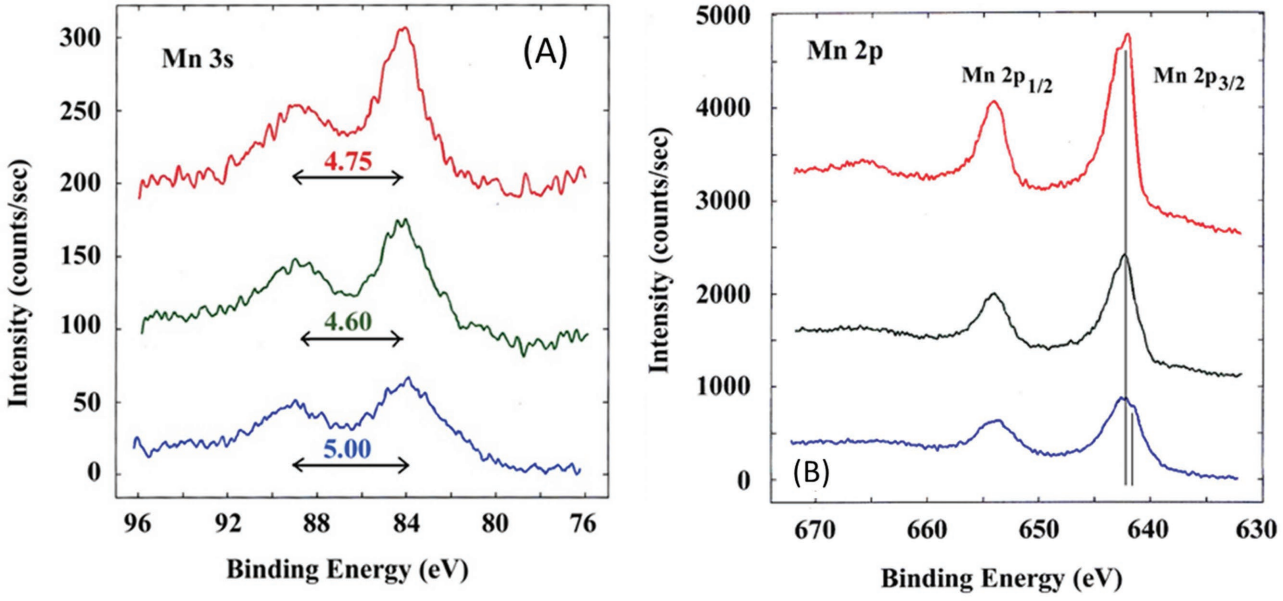

Figure 3. A) Mn 3s and B) Mn 2p XPS spectra of untreated pristine (red), 2 h NH_3 (green) and 4 h NH_3-treated (blue) Li-rich materials. The Mn 3s spectra include color-coded values for the magnitude of the splitting between the two peaks. The vertical lines for the Mn $2p_{3/2}$ spectra indicate a shift to higher binding energies for the Li-rich materials samples treated with NH_3 for 2 and 4 h.

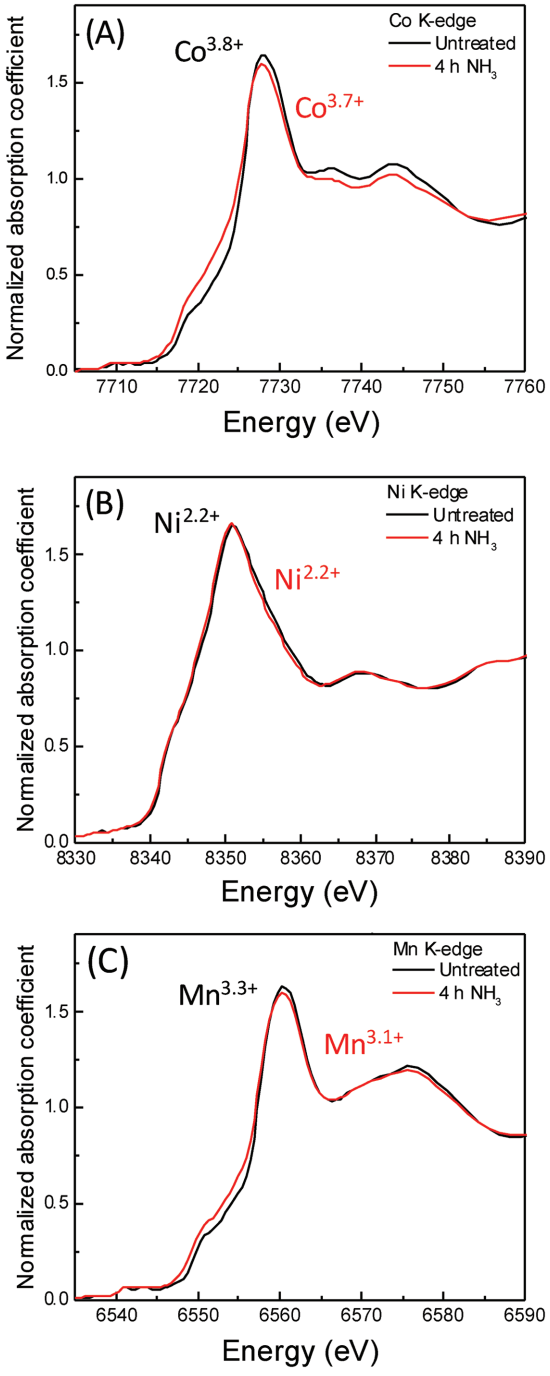

Figure 4. K-edge XANES data for A) Co, B) Ni, and C) Mn of the untreated and 4 h NH_3-treated Li-rich materials. The oxidation states of transition metals taken from edge shifts are indicated by color.

metal oxidation states are known to occur, such as disproportionation reactions, spinel formation, oxygen vacancy creation, or reaction with O_2 from the air after synthesis.[4,23,26]

Along with XPS and XANES, we also used Raman spectroscopy as a short-range order technique to probe the surface structure of cathode materials. **Figure 6** represents the Raman spectra of the 4 h NH_3-treated and untreated material. We have established that for the ammonia-treated material, the main Raman peak at 592 cm^{-1} of pristine sample splits into two or shifts to the right, to around 625 cm^{-1} (as detected from various locations on the sample). This blueshift is typical for the layered-to-spinel type ordering transformation upon cycling of layered structure electrode materials[39] and is established first in this work for the NH_3 gas treated Li-rich materials. The peak at 422 cm^{-1} disappears and a new minor peak at 154 cm^{-1} emerges that may relate to Li_2CO_3 species, although the main characteristic one (fingerprint) for Li_2CO_3 lies at 1090 cm^{-1}. We suppose that NH_3 treatment especially for 4 h (1 and 2 h exposure do not affect the Raman responses) causes changes in the surface layer of Li-rich materials, like minor Li leaching and O-release that trigger partial migration of Mn ions to the Li layer. This may result in some layered-to-spinel transition, or in a sort of oxygen-deficient intermediate structure. The following reactions are possible during NH_3 thermal treatment of lithiated transition metal oxide materials (for instance, Li_2MnO_3) as described in the literature[40,41]

$$2Li_2MnO_3 + NH_3 + 1.5O_{lattice}\,(\text{at } 400\,^{\circ}C) \rightarrow 2LiMnO_2 + Li_2O + 1.5H_2O + NO\uparrow \quad (1)$$

$$2Li_2MnO_3 + Li_2O + O_{lattice}\,(\text{at } 400\,^{\circ}C) \rightarrow 2LiMnO_2 + 2Li_2O_2 \quad (2)$$

These reactions result in partial reduction of Mn^{4+} ions detected by our XPS studies (Figure 3) and in formation of lithium oxide and peroxide species, as discussed below. Spinel can also be formed due to decomposition of $LiMnO_2$ into $LiMn_2O_4$ and Li_2MnO_3 at $T > 350$ °C.[41]

Figure 7 depicts the Fourier transform magnitudes of k^2-weighted K-edge EXAFS data of Ni, Co, and Mn for untreated and 4 h NH_3-treated Li-rich material. The first peak is assigned to the contribution from oxygen, and the second peak to the nearest metal neighbors. From visual observation, for both Mn and especially Co, the M—M and M—O peaks are greatly decreased after NH_3 treatment. It is also obtained from the analysis of EXAFS data at Co and Mn K-edge, that M—O coordination numbers reduce from 5.4 to 4.7 for Co, and 5.8 to 5.3 for Mn after NH_3 treatment, while the Ni—O peak amplitudes and positions for both samples are almost the same, as shown in Figure 7B. It is suggested from the fitting results that the reduced intensity of M—M peak for all three edges is due to the increase of disorder that is indicated by the Debye–Waller factor (σ^2) values which slightly increase after NH_3 treatment by ≈0.002 Å^2. It is shown from EXAFS data that NH_3 treatment affects the local structure of Co and Mn much more dramatically than that of Ni. The EXAFS fitting values for M—M and M—O coordination numbers, bond distances, and σ^2 values are presented in Table S1 (Supporting Information).

2.4. Evidence of Li^+ Extraction from Li-Rich Materials and Formation of Surface Lithium Salts after NH_3 Treatment

Figure 8 represents the XPS O 1s and C 1s structures of untreated and NH_3-treated materials. The results show that the lattice oxygen peak, marked in the figures as O in Li-rich

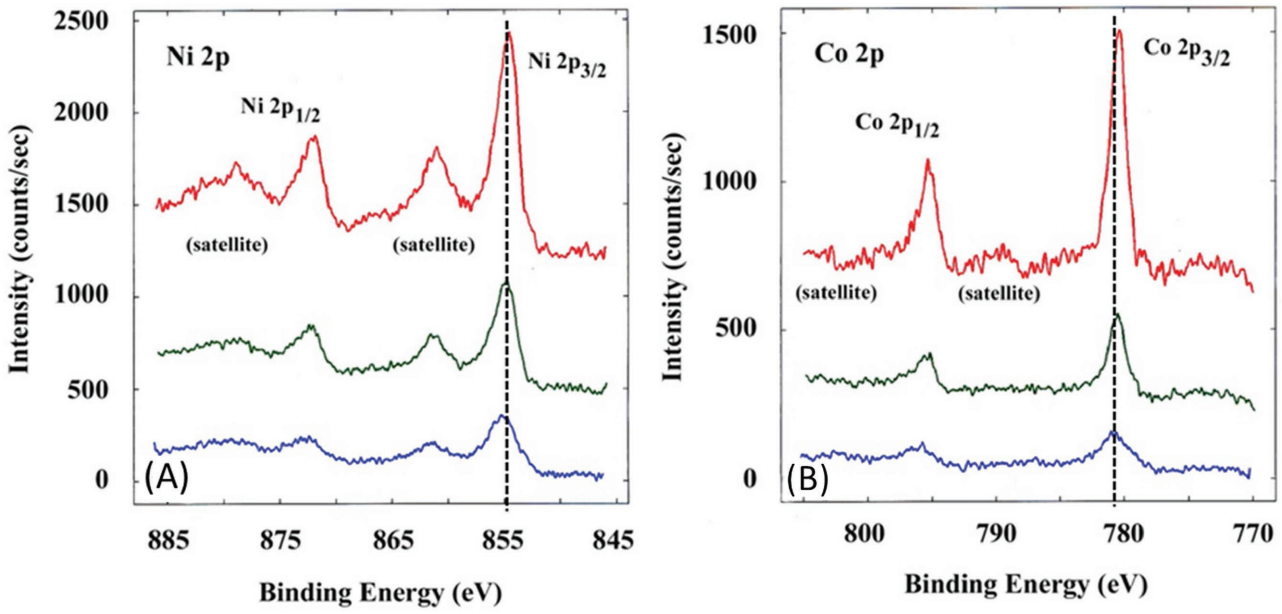

Figure 5. A) Ni and B) Co 2p XPS spectra of untreated pristine (red), 2 h NH_3 (green), and 4 h NH_3 (blue) treated Li-rich materials. Vertical dashed lines are included for a reference.

material (≈529.6 eV in the pristine material)[42] is shifted to higher binding energies when it is treated with NH_3. Both the 2 and 4 h NH_3-treated samples demonstrate the presence of LiOH and Li_2CO_3, observed at 531.28 and 532.02 eV, respectively.[43,44] While the former appears in pristine sample as well, the latter is observed after the NH_3 treatment only and hence, is characteristic of this processing. The LiOH peak can overlap with that of Li_2O_2,[45] though this unstable compound is unlikely to form. LiOH can easily form as a result of leaching of Li^+ from the surface, with O^{2-} extracted to maintain charge balance and with H^+ from NH_3 (vide supra). LiOH then can react with CO_2 in the air to produce Li_2CO_3. Additionally, LiOH is used as a lithium source when annealed with the precursor

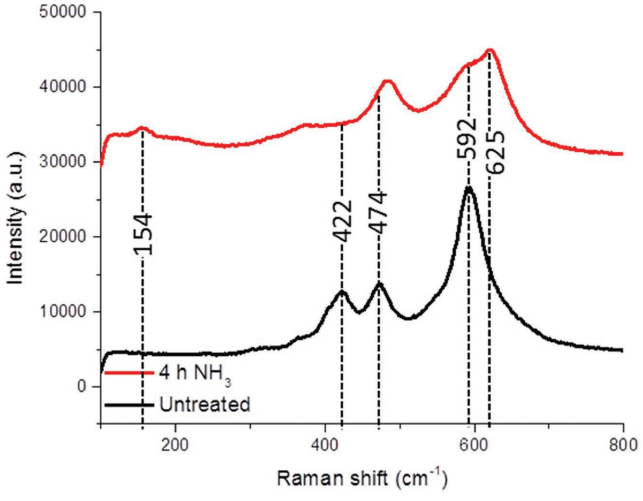

Figure 6. Typical Raman spectra of untreated and 4 h NH_3-treated Li-rich pristine (uncycled) materials.

material upon the Li-rich materials synthesis, so this is already present before treatment.

The Li_2O peak is present at 528.55 eV[43] for 4 h treated sample only. Curve fitting of the 4 h treated sample also resolves a peroxo-like component, in good agreement with a reported peroxo-like species attributed to oxidized $O_2^{\delta-}$ dimers.[16,46] All materials contain a characteristic C—O peak at ≈533 eV which is likely due to the carbon conductive tape that the material was adhered to during measurement.[47]

The amount of different oxygen containing species detected for untreated and NH_3-treated materials is indicated in Table S2 (Supporting Information). To note, the amount of oxygen from Li-rich material is lower with longer NH_3 treatment (67.5, 37.6, and 21.3 at% for untreated, 2 and 4 h NH_3-treated materials, respectively). It is likely that surface lattice oxygen of the oxide participates in the reaction with NH_3 creating thus O-vacancies accompanied with gas evolution, like NO and N_2.[40] Our TGA-MS experiments under N_2 showed that the Li-rich materials lost ≈1% weight in the form of H_2O, CO_2, and mostly O_2, with the treated material expelling more and absorbing less weight (Figure S1, Supporting Information). Expulsion of surface oxygen from Li-rich materials is known in the literature.[34]

Further evidence for carbonate formation is presented in the C 1s spectra (Figure 8D). The XPS peak for Li_2CO_3 (at about 288–289 eV) is enhanced greatly after NH_3 treatments. This is likely due to interactions of Li_2O and LiOH that form upon exposure to NH_3 with CO_2 in the atmosphere to create Li_2CO_3. This finding also correlates with our Raman spectroscopy data demonstrating lithium carbonate formation (Figure 6).

The total atomic percentages of several elements derived from XPS spectra are presented in Table S3 (Supporting Information). The Li and C percentages all increase with the NH_3 treatment time, indicative of the partial leaching of Li from the

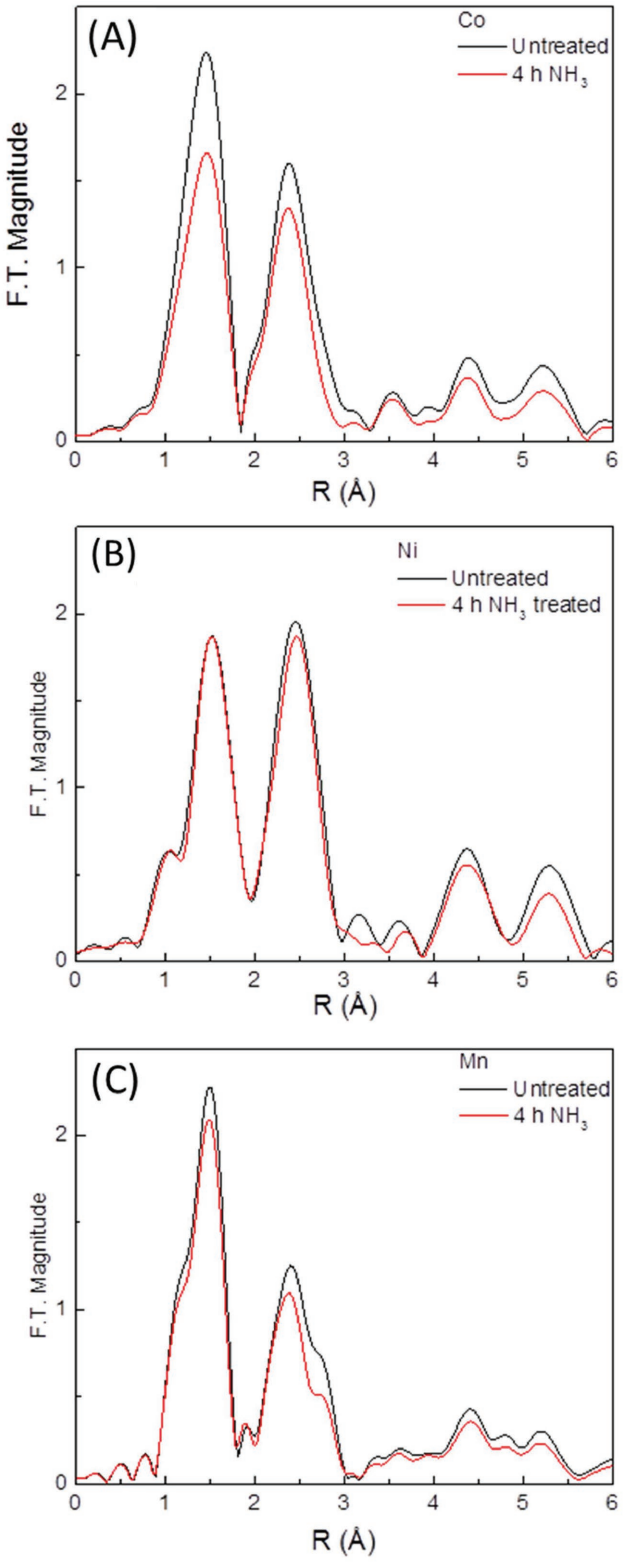

Figure 7. Fourier transform magnitudes of k^2-weighted K-edge EXAFS data of A) Co, B) Ni, and C) Mn for the untreated and 4 h NH_3-treated Li-rich materials.

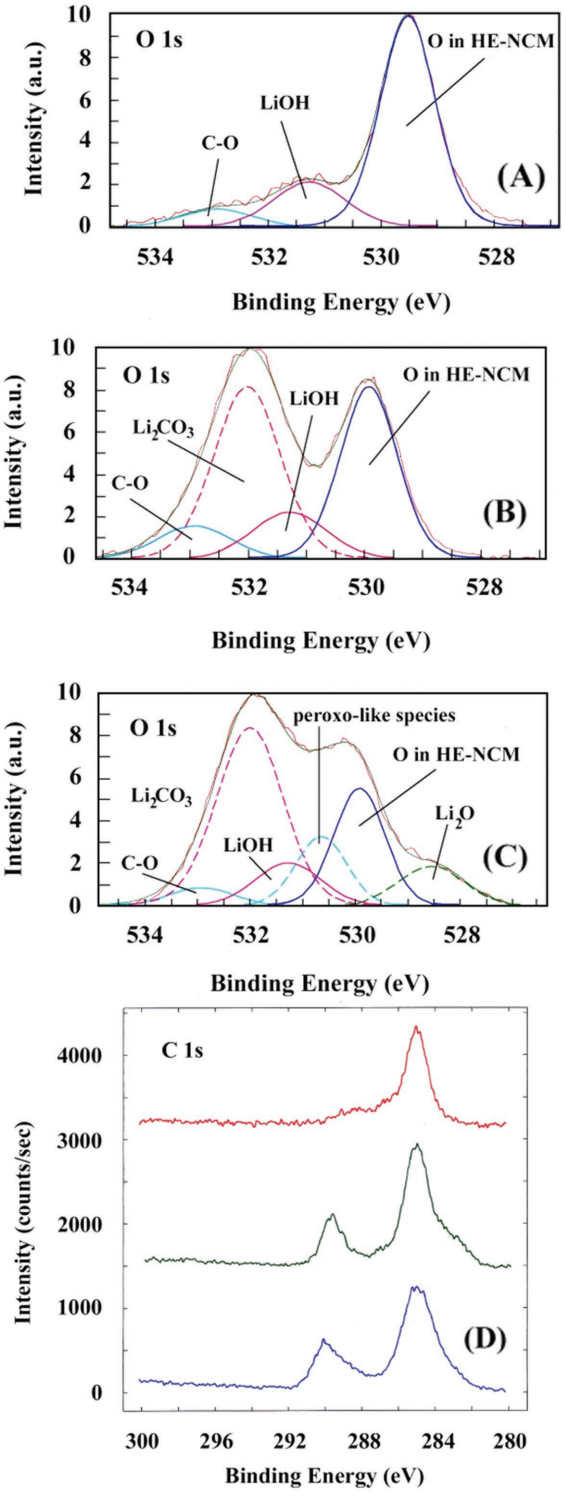

Figure 8. A) O 1s XPS spectra of the untreated, B) 2 h NH_3-treated, and C) 4 h NH_3-treated Li-rich materials. Curve fitting provides clear evidence for existence of various O-containing species (lattice oxygen, lithium oxide, peroxo-like species). D) C 1s peaks measured from the untreated (red), 2 h NH_3 (green), and 4 h NH_3 (blue) treated Li-rich materials (marked as high-energy $Li_{1+x}[Ni—Co—Mn]—O_2$) materials, HE-NCM).

surface and the reaction with the CO_2 in the atmosphere. The oxygen peak decreases slightly, indicating that some of the O expelled from the surface during the heating process may escape as molecular oxygen, which would make sense considering the 30 min preheating step of the materials at 400 °C under N_2 prior to exposing the material to NH_3 (as noted in the Experimental Section). It could be that further reaction of surface oxides with NH_3 is driven by the formation of H_2O and Li_2O.

Further evidence for a formation of surface Li containing species is found in the fact that as NH_3 treatment time is higher, the TM percentages decrease, which would occur when the particle surface is partially covered by the above species. An interesting fact is the presence of the nitrogen detected by XPS in the sample, which agrees with previous reports that some sort of nitridation can occur after exposure of TM oxides to NH_3, though the N-peak intensity we observed is much lower than in the work by Zhang et al.[27] XPS measurements have previously reported that species containing M—NH_2 and M—OH bonds may form upon exposure to NH_3, though these were unstable.[28] LiOH was also observed in XRD patterns of Li-rich material treated for 4 h by NH_3, indicating the high proportion of LiOH formed in the material (Figure S2, derived values in Table S4, Supporting Information). Electron diffraction patterns from transmission electron microscopy (TEM) measurements also show formation of LiOH and Li_2CO_3, agreeing with XRD and XPS data (Figure S3–S4, Supporting Information).

3. Conclusions

We have demonstrated in this work that NH_3 treatments of Li-rich materials at 400 °C improve discharge capacity of electrodes and decrease the fading of discharge capacity and average voltage during cycling in Li-cells. An optimal duration of the treatment was established as 2 h, resulting in modified Li-rich materials that provide stable performance with discharge capacities ≈220 mA h g^{-1} at a *C*/3 rate. The analysis of the electrochemical data (d*q*/d*V* plots) measured from ammonia-treated materials allowed us to suggest that treatment increases Li^+ insertion kinetics to the Li-layer at the expense of the TM layer in Li-rich material. This was evidenced from shifting of the corresponding redox potentials to lower values and their broadening that implies to slower electrochemical kinetics.

We have found no significant changes in the lattice parameters of the Li_2MnO_3 and Li(TM)O_2 phases of Li-rich materials as a result of treatment (see Table S4, Supporting Information), thus indicating that in fact the NH_3 treatment does not alter the material's bulk structure. However, we demonstrated for the first time that NH_3 treatment causes several important structural surface effects to Li-rich cathode materials, for instance:

(1) Partial reduction of Mn and Co that occurs through the surface and bulk of the material.
(2) A subtle structural change (not observed by XRD), which may include surface formation of an oxygen-deficient spinel-like phase due to partial layered-to-spinel transformation and to thermal reactions of ammonia with oxides.
(3) Formation of lithium oxides and salts at the surface of the material.

NH_3 oxidizes at the surface of the Li-rich particle's surface at 400 °C, partially reducing transition metals (confirmed by XPS and XANES studies) and forming, for instance, NO gas, as reported earlier.[40] Upon ammonia treatment, protons are generated from the NH_3, and the surface oxygen is removed to maintain charge balance as Li^+ is partially leached from the surface. Oxygen removal (around 1%) was established directly by TGA-MS studies of Li-rich material under pure nitrogen at 400 °C. From the Li^+ leached, LiOH and Li_2O are formed, which may convert to Li_2CO_3 upon exposure to CO_2 in the air. We suggest that the result of O^{2-} elimination from the particle surface is the formation of a spinel-like, oxygen-deficient phase.

Further work will be focused on studies of Li-rich materials in full cells versus graphite anodes, to evaluate if NH_3 treatment can indeed improve the likelihood of commercialization of the Li-rich materials in Li-ion batteries. In addition, preparation of a separate paper from our groups is under way dedicated to solid-state NMR studies of these materials thermally treated with ammonia.

4. Experimental Section

Materials and Treatment Procedure with NH_3: The Li-rich material, $0.35Li_2MnO_3{\cdot}0.65LiNi_{0.35}Mn_{0.45}Co_{0.20}O_2$ was synthesized at BASF. The NH_3 treatments were carried out at 400 °C in a temperature controlled oven. For the experiments, 50 g of material was exposed to NH_3 at a gas flow around 15 L h^{-1} over 1, 2, and 4 h. Prior to the NH_3 treatment, the materials were heated to 400 °C over 1.5 h, including a 0.5 h constant temperature plateau, under N_2.

Electrochemical Experiments: Composite electrodes were prepared using 80% active cathode Li-rich material, 5% Super P carbon black, 5% KS 6 graphite, and 10% PVDF (Solef 5130). The electrode loading was ≈3 mg cm^{-2}. Coin cells of 2325-type were fabricated with Li-metal counter electrodes, a Celgard 2500 polypropylene separator, and 3:7 ethylene carbonate–ethyl methyl carbonate, and 1 M $LiPF_6$ electrolyte solution (BASF). For all experiments, at least three coin cells were used, an average discharge capacity reported, and the standard deviation among cells used as error bars in the relevant figures. All cells were subjected to cycling at 30 °C, as follows: the first activation step was performed from OCV to 4.7 V in charge and to 2.0 V in discharge, at a *C*/15 rate, *C* defined as 250 mA h g^{-1}. All subsequent cycles were performed from 2 to 4.6 V. For the first cycle, a constant voltage step of 3 h was applied at the anodic limit; all subsequent constant voltage steps were for 30 min. After the initial *C*/15 formation cycle, two cycles at *C*/10 were performed, followed by three cycles at *C*/3, 0.8*C*, 1*C*, 2*C*, 4*C*, and 0.1*C*, after which 80 cycles were performed at *C*/3 and then the cycling was terminated.

Characterization Techniques: XPS, XRD, Raman Spectroscopy, X-Ray Absorption Fine Structure (XAFS), TEM, Electron Diffraction, and TGA: XPS measurements were carried out using 5600 Multi-Technique System (PHI, USA) with Al Kα monochromated source (1486.6 eV). The binding energy of adventitious carbon at 285.0 eV was taken as an energy reference for all measured peaks. High-resolution spectra were taken at pass energy of 11.75 eV and at increments of 0.05 eV $step^{-1}$. Curve fitting was done with Gaussian–Lorentzian function by using a 5600 Multi-Technique System software. Two fitting parameters, peak position and full width at half-maximum, were fixed within less than about ±0.2 eV.

For XRD measurements, a Bruker D8 Advanced X-ray diffractometer using CuKα radiation was employed. The intensities were recorded within the 2θ range from 10° to 80° with 2θ steps of ≈0.0194° from powder samples. The cell parameters were obtained from the data by a standard least squares refinement procedure.

Micro-Raman spectroscopy measurements were performed at room temperature using a micro-Raman spectrometer from Renishaw inVia (UK) equipped with a 514 nm laser, a CCD camera, and an optical Leica microscope. A 50× objective lens to focus the incident beam and an 1800 lines mm- grating were used. The diameter of the laser beam was ≈1 µm. For statistical purposes, at least 10–15 locations were measured from a sample.

XAFS spectroscopy measurements, including XANES and EXAFS, were performed on the untreated and 4 h NH_3-treated (blue) Li-rich materials. The Ni, Co, and Mn K-edge XAFS data were collected in transmission mode at Advanced Photon Source (APS) 10BM-A,B beamline using a Si(111) double-crystal monochromator. Samples were ground to fine powders and spread on tape with a brush for measurements. At least two scans were taken for each edge for averaging. XAFS data processing and analysis were done using the Athena and Artemis software within the IFEFFIT package.[48] The positions of absorption edge in Li-rich materials were compared with their respective foil and oxide standards to estimate the average charge state of transition metals (Ni, Co, and Mn) in the samples, using a linear approximation.[37] The absorption edge position here was defined by the first inflection point of the absorption edge. The normalized k^2-weighted EXAFS data were Fourier transformed using the k range of 2–12 Å^{-1} for Ni, 2–13 Å^{-1} for Mn, and 2–11 Å^{-1} for Co. To fit the EXAFS data, the contributions from metal–oxygen (M—O) and metal–metal (M—M) paths, assuming the $LiNiO_2$ structure, were included in the theoretical EXAFS spectrum. The values of the amplitude reduction factor (S_0^2) for Co, Ni, or Mn were obtained from the fitting of the corresponding metal foil and fixed in the fits to the Li-rich materials.

TEM examinations were carried out with a LaB_6-200 kV Jeol-2100 transmission electron microscope operated at 200 kV. A unique identification of the structures was based on the analysis of the convergent nanobeam electron diffraction patterns obtained with a 7 nm probe size. Specimens of Li-rich materials for observation in TEM were prepared onto lacey carbon grids as described previously.[4,49] TEM images and nanobeam electron diffraction patterns were collected from various particles in the samples.

Supporting Information

Supporting Information is available from the Wiley Online Library or from the author.

Acknowledgements

D.A. thanks and acknowledges BASF SE for funding. B.M. thanks Mr. Gregory Avrushenko for his help in maintaining the NH_3 gas treatment apparatus and useful discussions. A.I.F. and J.L. acknowledge support by the U.S. National Science Foundation Grant No. CHE-1413937. MRCAT operations are supported by the Department of Energy and the MRCAT member institutions. This research used resources of the Advanced Photon Source, a U.S. Department of Energy (DOE) Office of Science User Facility operated for the DOE Office of Science by Argonne National Laboratory under Contract No. DE-AC02-06CH11357.

Conflict of Interest

The authors declare no conflict of interest.

Keywords

ammonia treatment, cathodes, lithium-ion batteries, lithium-rich materials, stabilization, voltage fade

Received: March 15, 2017
Revised: April 3, 2017
Published online: May 22, 2017

[1] M. H. Rossouw, M. M. Thackeray, *Mater. Res. Bull.* **1991**, *26*, 463.
[2] P. Kalyani, S. Chitra, T. Mohan, S. Gopukumar, *J. Power Sources* **1999**, *80*, 103.
[3] M. M. Thackeray, C. S. Johnson, J. T. Vaughey, N. Li, S. A. Hackney, *J. Mater. Chem.* **2005**, *15*, 2257.
[4] S. F. Amalraj, B. Markovsky, D. Sharon, M. Talianker, E. Zinigrad, R. Persky, O. Haik, J. Grinblat, J. Lampert, M. Schulz-Dobrick, A. Garsuch, L. Burlaka, D. Aurbach, *Electrochim. Acta* **2012**, *78*, 32.
[5] a) T. Ohzuku, A. Ueda, M. Nagayama, *J. Electrochem. Soc.* **1993**, *140*, 1862; b) E. Zhecheva, R. Stoyanova, R. Alcantara, P. Lavela, J. L. Tirado, *Pure Appl. Chem.* **2002**, *74*, 1885.
[6] a) A. R. Armstrong, P. G. Bruce, *Nature* **1996**, *381*, 499; b) F. Capitaine, P. Gravereau, C. Delmas, *Solid State Ionics* **1996**, *89*, 197.
[7] a) L. Croguennec, P. Deniard, R. Brec, *J. Electrochem. Soc.* **1997**, *144*, 3323; b) S.-H. Wu, M.-T. Yu, *J. Power Sources* **2007**, *165*, 660; c) F. Schipper, E. M. Erickson, C. Erk, J.-Y. Shin, F. F. Chesneau, D. Aurbach, *J. Electrochem. Soc.* **2017**, *164*, A6220; d) F. Schipper, D. Aurbach, *Russ. J. Electrochem.* **2016**, *52*, 1095.
[8] a) C. S. Johnson, S. D. Korte, J. T. Vaughey, M. M. Thackeray, T. E. Bofinger, Y. Shao-Horn, S. A. Hackney, *J. Power Sources* **1999**, *81*, 491; b) T. Ohzuku, Y. Makimura, *Chem. Lett.* **2001**, *30*, 642.
[9] a) J.-S. Kim, C. S. Johnson, J. T. Vaughey, M. M. Thackeray, S. A. Hackney, W. Yoon, C. P. Grey, *Chem. Mater.* **2004**, *16*, 1996; b) Y. Wu, A. Manthiram, *Electrochem. Solid-State Lett.* **2006**, *9*, A221; c) S. H. Kang, K. Amine, *J. Power Sources* **2005**, *146*, 654.
[10] M. M. Thackeray, C. S. Johnson, K. Amine, J. Kim, *Google Patents*, **2004**.
[11] C. Johnson, S. H. Kang, M. Thackeray, *Google Patents*, **2006**.
[12] C. S. Johnson, N. Li, C. Lefief, J. T. Vaughey, M. M. Thackeray, *Chem. Mater.* **2008**, *20*, 6095.
[13] C. S. Johnson, N. Li, C. Lefief, M. M. Thackeray, *Electrochem. Commun.* **2007**, *9*, 787.
[14] C. Yu, G. Li, X. Guan, J. Zheng, D. Luo, L. Li, *Phys. Chem. Chem. Phys.* **2012**, *14*, 12368.
[15] D. Mohanty, S. Kalnaus, R. A. Meisner, K. J. Rhodes, J. L. Li, E. A. Payzant, D. L. Wood, C. Daniel, *J. Power Sources* **2013**, *229*, 239.
[16] E. McCalla, A. M. Abakumov, M. Saubanere, D. Foix, E. J. Berg, G. Rousse, M.-L. Doublet, D. Gonbeau, P. Novak, G. Van Tendeloo, R. Dominko, J.-M. Tarascon, *Science* **2015**, *350*, 1516.
[17] E. McCalla, M. T. Sougrati, G. Rousse, E. J. Berg, A. Abakumov, N. Recham, K. Ramesha, M. Sathiya, R. Dominko, G. Van Tendeloo, P. Novak, J.-M. Tarascon, *J. Am. Chem. Soc.* **2015**, *137*, 4804.
[18] M. Sathiya, A. M. Abakumov, D. Foix, G. Rousse, K. Ramesha, M. Saubanere, M. L. Doublet, H. Vezin, C. P. Laisa, A. S. Prakash, D. Gonbeau, G. VanTendeloo, J. M. Tarascon, *Nat. Mater.* **2015**, *14*, 230.
[19] P. Rozier, J. M. Tarascon, *J. Electrochem. Soc.* **2015**, *162*, A2490.
[20] a) E. M. Erickson, F. Schipper, R. Tian, J.-Y. Shin, C. Erk, F. F. Chesneau, J. K. Lampert, B. Markovsky, D. Aurbach, *RSC Adv.* **2017**, *7*, 7116; b) A. Watanabe, F. Matsumoto, M. Fukunishi, G. Kobayashi, A. Ito, M. Hatano, Y. Ohsawa, Y. Sato, *Electrochemistry* **2012**, *80*, 561; c) A. Ito, D. Li, Y. Ohsawa, Y. Sato, *J. Power Sources* **2008**, *183*, 344.

[21] a) E. M. Erickson, F. Schipper, R. Tian, J.-Y. Shin, C. Erk, F.-F. Chesneau, J. Lampert, B. Markovsky, D. Aurbach, *RSC Adv.* **2017**, *7*, 12, 7116; b) K. Kang, G. Ceder, *Phys. Rev. B* **2006**, *74*, 094105; c) F. Amalraj, M. Talianker, B. Markovsky, L. Burlaka, N. Leifer, G. Goobes, E. M. Erickson, O. Haik, J. Grinblat, E. Zinigrad, D. Aurbach, J. K. Lampert, J.-Y. Shin, M. Schulz-Dobrick, A. Garsuch, *J. Electrochem. Soc.* **2013**, *160*, A2220.

[22] E. M. Erickson, F. Schipper, T. R. Penki, J.-Y. Shin, C. Erk, F.-F. Chesneau, B. Markovsky, D. Aurbach, *J. Electrochem. Soc.* **2017**, *164*, A6341.

[23] J. Reed, G. Ceder, *Chem. Rev.* **2004**, *104*, 4513.

[24] E. M. Erickson, C. Ghanty, D. Aurbach, *J. Phys. Chem. Lett.* **2014**, *5*, 3313.

[25] M. N. Richard, E. W. Fuller, J. R. Dahn, *Solid State Ionics* **1994**, *73*, 81.

[26] B. Qiu, M. Zhang, L. Wu, J. Wang, Y. Xia, D. Qian, H. Liu, S. Hy, Y. Chen, K. An, Y. Zhu, Z. Liu, Y. S. Meng, *Nat. Commun.* **2016**, *12108*, 7.

[27] H. Z. Zhang, Q. Q. Qiao, G. R. Li, S. H. Ye, X. P. Gao, *J. Mater. Chem.* **2012**, *22*, 13104.

[28] N. Andreu, D. Flahaut, R. Dedryvere, M. Minvielle, H. Martinez, D. Gonbeau, *ACS Appl. Mater. Interfaces* **2015**, *7*, 6629.

[29] a) J. R. Croy, K. G. Gallagher, M. Balasubramanian, B. R. Long, M. M. Thackeray, *J. Electrochem. Soc.* **2014**, *161*, A318; b) K. G. Gallagher, J. R. Croy, M. Balasubramanian, M. Bettge, D. P. Abraham, A. K. Burrell, M. M. Thackeray, *Electrochem. Commun.* **2013**, *33*, 96.

[30] X. Yu, Y. Lyu, L. Gu, H. Wu, S.-M. Bak, Y. Zhou, K. Amine, S. N. Ehrlich, H. Li, K.-W. Nam, X.-Q. Yang, *Adv. Energy Mater.* **2014**, *4*, 1300950.

[31] a) Z. Lu, J. R. Dahn, *J. Electrochem. Soc.* **2002**, *149*, A815; b) C. R. Fell, M. Chi, Y. S. Meng, J. L. Jones, *Solid State Ionics* **2012**, *207*, 44.

[32] C. Ghanty, B. Markovsky, E. M. Erickson, M. Talianker, O. Haik, Y. Tal-Yossef, A. Mor, D. Aurbach, J. Lampert, A. Volkov, J.-Y. Shin, A. Garsuch, F. F. Chesneau, C. Erk, *ChemElectroChem* **2015**, *2*, 1479.

[33] a) J. R. Croy, D. Kim, M. Balasubramanian, K. Gallagher, S. H. Kang, M. M. Thackeray, *J. Electrochem. Soc.* **2012**, *159*, A781; b) H. J. Yu, H. J. Kim, Y. R. Wang, P. He, D. Asakura, Y. Nakamura, H. S. Zhou, *Phys. Chem. Chem. Phys.* **2012**, *14*, 6584; c) M. N. Ates, S. Mukerjee, K. M. Abraham, *RSC Adv.* **2015**, *5*, 27375.

[34] a) P. Yan, L. Xiao, J. Zheng, Y. Zhou, Y. He, X. Zu, S. X. Mao, J. Xiao, F. Gao, J.-G. Zhang, C.-M. Wang, *Chem. Mater.* **2015**, *27*, 975; b) A. Boulineau, L. Simonin, J.-F. Colin, C. Bourbon, S. Patoux, *Nano Lett.* **2013**, *13*, 3857.

[35] a) M. Saubanere, E. McCalla, J. M. Tarascon, M. L. Doublet, *Energy Environ. Sci.* **2016**, *9*, 984; b) E. McCalla, A. S. Prakash, E. Berg, M. Saubanere, A. M. Abakumov, D. Foix, B. Klobes, M.-T. Sougrati, G. Rousse, F. Lepoivre, S. Mariyappan, M.-L. Doublet, D. Gonbeau, P. Novak, G. Van Tendeloo, R. P. Hermann, J.-M. Tarascon, *J. Electrochem. Soc.* **2015**, *162*, A1341; c) M. Sathiya, G. Rousse, K. Ramesha, C. P. Laisa, H. Vezin, M. T. Sougrati, M. L. Doublet, D. Foix, D. Gonbeau, W. Walker, A. S. Prakash, M. Ben Hassine, L. Dupont, J. M. Tarascon, *Nat. Mater.* **2013**, *12*, 827.

[36] M. C. Biesinger, B. P. Payne, A. P. Grosvenor, L. W. M. Lau, A. R. Gerson, R. S. C. Smart, *Appl. Surf. Sci.* **2011**, *257*, 2717.

[37] a) S. J. A. Figueroa, F. G. Requejo, E. J. Lede, L. Lamaita, M. A. Peluso, J. E. Sambeth, *Catal. Today* **2005**, *107*, 849; b) W. E. O'Grady, K. I. Pandya, K. E. Swider, D. A. Corrigan, *J. Electrochem. Soc.* **1996**, *143*, 1613; c) J. Wong, F. W. Lytle, R. P. Messmer, D. H. Maylotte, *Phys. Rev. B* **1984**, *30*, 5596.

[38] A. P. Grosvenor, M. C. Biesinger, R. S. C. Smart, N. S. McIntyre, *Surf. Sci.* **2006**, *600*, 1771.

[39] a) P. K. Nayak, J. Grinblat, M. Levi, B. Markovsky, D. Aurbach, *J. Electrochem. Soc.* **2014**, *161*, A1534; b) P. K. Nayak, J. Grinblat, E. Levi, B. Markovsky, D. Aurbach, *J. Power Sources* **2016**, *318*, 9.

[40] J. Pérez-Ramírez, E. V. Kondratenko, *J. Catal.* **2007**, *250*, 240.

[41] J. Molenda, M. Ziemnicki, M. Molenda, M. Bucko, J. Marzec, *Mater. Sci. Poland* **2006**, *24*, 75.

[42] A. M. Andersson, D. P. Abraham, R. Haasch, S. MacLaren, J. Liu, K. Amine, *J. Electrochem. Soc.* **2002**, *149*, A1358.

[43] a) K. Kanamura, H. Tamura, Z.-I. Takehara, *J. Electroanal. Chem.* **1992**, *333*, 127; b) K. P. C. Yao, D. G. Kwabi, R. A. Quinlan, A. N. Mansour, A. Grimaud, Y.-L. Lee, Y.-C. Lu, Y. Shao-Horn, *J. Electrochem. Soc.* **2013**, *160*, A824.

[44] S. Mizuno, H. Tochihara, T. Kadowaki, H. Minagawa, K. Hayakawa, I. Toyoshima, C. Oshima, *Surf. Sci.* **1992**, *264*, 103.

[45] R. Younesi, M. Hahlin, F. Björefors, P. Johansson, K. Edström, *Chem. Mater.* **2013**, *25*, 77.

[46] D. Foix, M. Sathiya, E. McCalla, J.-M. Tarascon, D. Gonbeau, *J. Phys. Chem. C* **2016**, *120*, 862.

[47] H. Hantsche, *Adv. Mater.* **1993**, *5*, 778.

[48] a) B. Ravel, M. Newville, *J. Synchrotron Radiat.* **2005**, *12*, 537; b) M. Newville, *J. Synchrotron Radiat.* **2001**, *8*, 322.

[49] a) D. Aurbach, O. Srur-Lavi, C. Ghanty, M. Dixit, O. Haik, M. Talianker, Y. Grinblat, N. Leifer, R. Lavi, D. T. Major, G. Goobes, E. Zinigrad, E. M. Erickson, M. Kosa, B. Markovsky, J. Lampert, A. Volkov, J.-Y. Shin, A. Garsuch, *J. Electrochem. Soc.* **2015**, *162*, A1014; b) O. Haik, N. Leifer, Z. Samuk-Fromovich, E. Zinigrad, B. Markovsky, L. Larush, Y. Goffer, G. Goobes, D. Aurbach, *J. Electrochem. Soc.* **2010**, *157*, A1099; c) F. Amalraj, D. Kovacheva, M. Talianker, L. Zeiri, J. Grinblat, N. Leifer, G. Goobes, B. Markovsky, D. Aurbach, *J. Electrochem. Soc.* **2010**, *157*, A1121.

